CHIN. PHYS. LETT. Vol. 38, No. 11 (2021) 117201

Enhanced Thermoelectric Properties of Cu_xSe ($1.75 \leq x \leq 2.10$) during Phase Transitions

Zhongmou Yue(岳仲谋)[1,2], Kunpeng Zhao(赵琨鹏)[3*], Hongyi Chen(陈弘毅)[4], Pengfei Qiu(仇鹏飞)[1,2], Lidong Chen(陈立东)[1,2], and Xun Shi(史迅)[1,2*]

[1]*State Key Laboratory of High Performance Ceramics and Superfine Microstructure, Shanghai Institute of Ceramics, Chinese Academy of Sciences, Shanghai 200050, China*

[2]*Center of Materials Science and Optoelectronics Engineering, University of Chinese Academy of Sciences, Beijing 100049, China*

[3]*State Key Laboratory of Metal Matrix Composites, School of Materials Science and Engineering, Shanghai Jiao Tong University, Shanghai 200240, China*

[4]*College of Chemistry and Chemical Engineering, Central South University, Changsha 410083, China*

(Received 26 August 2021; accepted 17 September 2021; published online 27 October 2021)

Coupling of a phase transition to electron and phonon transports provides extra degree of freedom to improve the thermoelectric performance, while the pertinent experimental and theoretical studies are still rare. Particularly, the impaction of chemical compositions and phase transition characters on the abnormal thermoelectric properties across phase transitions are largely unclear. Herein, by varying the Cu content x from 1.75 to 2.10, we systemically investigate the crystal structural evolution, phase transition features, and especially the thermoelectric properties during the phase transition for Cu_xSe. It is found that the addition of over-stoichiometry Cu in Cu_xSe could alter the phase transition characters and suppress the formation of Cu vacancies. The critical scatterings of phonons and electrons during phase transitions strongly enhance the Seebeck coefficient and diminish the thermal conductivity, leading to an ultrahigh dimensionless thermoelectric figure of merit of ∼1.38 at 397 K in $Cu_{2.10}Se$. With the decreasing Cu content, the critical electron and phonon scattering behaviors are mitigated, and the corresponding thermoelectric performances are reduced. This work offers inspirations for understanding and tuning the thermoelectric transport properties during phase transitions.

DOI: 10.1088/0256-307X/38/11/117201

Thermoelectric (TE) technology enables direct energy conversion between heat and electricity based on the Seebeck effect and Peltier effect.[1–3] Near-room-temperature solid-state heat pumps made from TE materials have attracted considerable interest by the electronic industry due to its ability in quickly cooling micro-processors, chips, and sensors.[4–7] The cooling capability of a TE device largely relies on the material's performance, which is mainly gauged by the dimensionless TE figure of merit, $zT = S^2T/\rho\kappa$, where S is the Seebeck coefficient, ρ is the electrical resistivity, κ is the thermal conductivity, and T is the absolute temperature. Over the past several decades, substantial efforts have been devoted to exploration and development of near-room-temperature TE materials. A series of promising TE materials with high performance have been discovered, such as MgAgSb,[8] Mg_3Bi_2,[9,10] Ag_2(Se/S/Te),[11–17] and nanostructured Bi_2Te_3[18–20] materials. However, most of these materials contain elements with high cost, high reactivity, or causticity. Bi_2Te_3-based materials are still the only TE material system that be widely used in commercial applications.[21] Developing novel high-performance and low-cost TE materials near room temperature is of momentous significance for the widespread use of TE cooling technology.

The traditional research paradigm of TEs usually focuses on the exploration of materials with ordered and static crystal structures, which limits the regulation of electron and phonon transports. With the change of external temperature or pressure, some materials undergo phase transformations, during which large atomic migration, dynamic fluctuations or reconstructions are involved.[22–25] This may cause strong critical scattering of phonons and electrons and thus induce phonon softening and band broadening.[26,27] These new phenomena and effects are distinct from the conventional TE transport behavior, providing a new tuning knob to decouple the thermal and electrical transports toward higher performance.[28,29]

Supported by the National Key Research and Development Program of China (Grant No. 2018YFB0703600), the National Natural Science Foundation of China (Grant Nos. 91963208, 51625205, 51961135106, and 51902199), Shanghai Government (Grant No. 20JC1415100), the CAS-DOE Program of Chinese Academy of Sciences (Grant No. 121631KYSB20180060), and the Shanghai Sailing Program (Grant No. 19YF1422800).

*Corresponding authors. Email: zkp.1989@sjtu.edu.cn; xshi@mail.sic.ac.cn.

© 2021 Chinese Physical Society and IOP Publishing Ltd

Copper selenide (Cu_2Se) semiconductor, a well-known liquid-like TE material,[30–39] is featured by an order-disorder phase transition at around 400 K.[22,24,26–28,30,40–46] At room temperature, Cu_2Se has a layered crystal structure (α-Cu_2Se) with Cu atoms alternately distributed at interlayers of the slightly distorted face-centered-cubic (fcc) Se sublattice [see Fig. 1(a)]. With increasing the temperature, a portion of Cu migrates from the copper rich to the copper deficient layer, transforming into a disordered antifluorite cubic structure (β-Cu_2Se) above 400 K [see Fig. 1(c)].[42] Such a structural transformation process has been reported as both the second- and the first-order phase transition.[22,24,28,43,47] Liu *et al.* firstly reported the abnormal TE properties of Cu_2Se during phase transitions.[22] They found that the measured thermal diffusivity and electrical conductivity can be greatly decreased, while the Seebeck coefficient can be sharply improved as the temperature approaches the phase transition point of Cu_2Se. The similar phenomenon was subsequently observed by several other groups.[26,43,45,46,48] A peak zT of 2.3 was attained when the Dulong–Petit heat capacity was used to calculate the thermal conductivity κ.[28] Chen *et al.* pointed out that the extraction of the true κ should exclude the heat exchange term from phase transition.[41] As such, the maximum zT value during phase transition was corrected to be 0.86, which is still three times higher than the normal phases.[41] Apart from the anomalous κ, the underlying mechanism behind the enhancement of S during phase transition remains an open issue. Liu *et al.* suggested that the extra enhancement of S in Cu_2Se could be induced by the critical scattering of electrons, which strongly alters the carrier mobility and its energy dependency.[28] Brown *et al.* surmised that the improvement of S may be caused by the entropy increment stemming from the rearrangement of Cu ions during phase transition.[48] Mahan *et al.* believed the cation disorder broadened the band energy and thus gave rise to the anomalous S.[26] Most recently, Sun *et al.* investigated the temperature dependent electronic structure of Cu_2Se using high-resolution angle-resolved photoemission spectroscopy.[27] They found that the electronic states were gradually changed when heating across the phase transition, which played a key role in the drastic temperature evolution of S.

As stated widely in literature, no unified understanding or conclusion has yet been reached. More efforts, including both theoretical and experimental studies, are needed to provide a more complete picture for these unusual properties. However, most previous works mainly focused on the theoretical investigation, while the experimental studies on the transport properties during phase transition are very rare. Particularly, the TE properties of Cu deficient or Cu excess Cu_xSe ($1.75 \leq x \leq 2.10$) during phase transition have not yet been reported up to date. As the Cu content has a large impact on both the phase transition characters and the thermoelectric properties, Cu_xSe thus offers a good example to systematically investigate the role of chemical composition on the electron and phonon transports during phase transitions.

In this work, via a routine melting-annealing recipe, we successfully synthesized a series of Cu_xSe samples with x ranging from 1.75 to 2.10. The influence of Cu content on the crystal structures, phase transition characters, and TE properties during phase transitions are systematically investigated. In particular, the relevant mechanisms of phonon and electron transports during the structural transformation processes are deeply discussed and analyzed. We believe this work provides new insights for understanding and engineering the TE properties during phase transitions.

Experiment. Polycrystalline Cu_xSe (x = 1.75, 1.80, 1.85, 1.90, 1.95, 2.00, 2.03 and 2.10) samples were prepared from high purity elements: Cu (shots, 99.999%, Alfa Aesar) and Se (shots, 99.999%, Alfa Aesar). The mixture of elements with different Cu/Se atomic ratios were weighted out according to the nominal chemical compositions. Then the mixture was loaded in a pyrolytic boron nitride crucible and sealed in silica tubes under vacuum. Subsequently, the tubes were heated up to 1423 K in 12 h and held at this temperature for 12 h, then cooled to 923 K over 48 h and followed by an annealing process over six days. A few Cu metal whiskers were observed on the surface of Cu_xSe ($x \geq 2.0$) ingots, which were removed before sintering. The ingots were handed ground to fine powders in an agate mortar and sintered by a spark plasma sintering facility (SPS, Sumitomo SPS-2040) at 673 K for 8 min under a pressure of 65 MPa. To reduce the impact of electrical current, the inner surface of the carbon dies was coated with electrically insulating BN layers to prevent the Cu migration during the sintering process. The relative densities of all samples were above 98%.

The crystal structures of synthesised Cu_xSe samples were examined by powder x-ray diffraction (PXRD, Rint 2000, Rigaku, Japan) using Cu K_α source (λ = 1.5405 Å) at room temperature and at 450 K. The scan speed is 2°/min and the scan step is 0.02°. The actual chemical composition of the sintered pellets was analyzed using field emission scanning electron microscopy (SEM, ZEISS SUPRA 55) equipped with energy dispersive microscopy (EDS, OXFORD Aztec XMax80). The differential scanning calorimetry (DSC) measurements were performed on Netzsch 200F3 with aluminium pans. To calculate the speed of

phase transition, all samples were subjected to heating rates of 1.0, 2.0, 5.0, 10.0 K/min. The thermal diffusivity was measured (λ_m) by the laser flash method (Netzsch LFA457) under continuous argon flow. The temperature interval was set to be as small as 1 K during the phase transition region. The sample density d was measured by the Archimedes method. As mentioned previously, the thermal conductivity during the phase transition should be calculated by $\kappa = C_{p0} \times d \times \lambda_0$, where C_{p0}, λ_0 are the heat capacity and thermal diffusivity without phase transition contribution, respectively. The measured heat capacity C_p could be divided into two parts: one is the normal heat capacity (C_{p0}) from phonons and electrons without the contribution from phase transition, and the other is the extra energy (C_{pt}) required to transform the low-temperature trigonal phase to high-temperature cubic phase. Therefore, by subtracting C_{pt} from the measured C_p, we can obtain the value of C_{p0}, which is also close to the theoretical Dulong–Petit value. The Seebeck coefficient S and electrical resistivity ρ during phase transitions were measured using a home-made measurement system based on the thermal expansion system (Netzsch DIL 402C) with a heating rate of 0.1 K/min. The electrical properties before and after the phase transitions were re-measured using a commercial apparatus ZEM-3 (ULVAC) to authenticate the data. Uncertainties in the electrical resistivity, Seebeck coefficient, and thermal diffusivity were ±4–9, ±4, and ±5–10%, respectively.[49] Hall coefficient (R_H) measurements were performed on a physical property measurement system (PPMS, Quantum Design) with magnetic field sweeping from −3 T to 3 T. The Hall carrier concentration p and carrier mobility μ were calculated by $p = 1/(eR_H)$ and $\mu = \sigma R_H$, respectively.

Results and Discussion. Figure 1(d) shows the room-temperature powder x-ray diffraction patterns for Cu_xSe (x = 1.75, 1.80, 1.85, 1.90, 1.95, 2.00, 2.03 and 2.10) samples. Clearly, the phase structures of Cu_xSe are very sensitive to their chemical compositions. All the diffraction peaks can be indexed to the trigonal structure of α-Cu_2Se (ICSD-4321181) when the nominal Cu content $x \geq 2.0$. With the decreasing Cu content, the diffraction peaks belonging to cubic β-Cu_2Se phase ($Fm\bar{3}m$, ICSD-150758) gradually increase, indicating a mixture of α- and β-$Cu_{2-x}Se$ phases in the region of $1.90 \leq x \leq 1.95$. However, with further decreasing the Cu content, the diffraction peaks of α-Cu_2Se phase disappear, while the remaining peaks well match with the β-Cu_2Se phase. An impurity phase of Cu_3Se_2 (ICSD-16949) is observed for $Cu_{1.75}Se$. These results agree well with the data from previous studies[50] and the Cu–Se binary diagram proposed by Heyding.[51] Note that a small amount of Cu metal whiskers was observed on the surface of the ingots of Cu_xSe with $x \geq 2.0$, which were removed before spark plasma sintering. Thus, the measured chemical composition of $x \geq 2.0$ pellets may deviate from their nominal ones, while the other samples have compositions closing to the nominal contents, as corroborated by our energy dispersive spectroscopy (EDS) results (see Fig. S1 in the Supplementary Material).

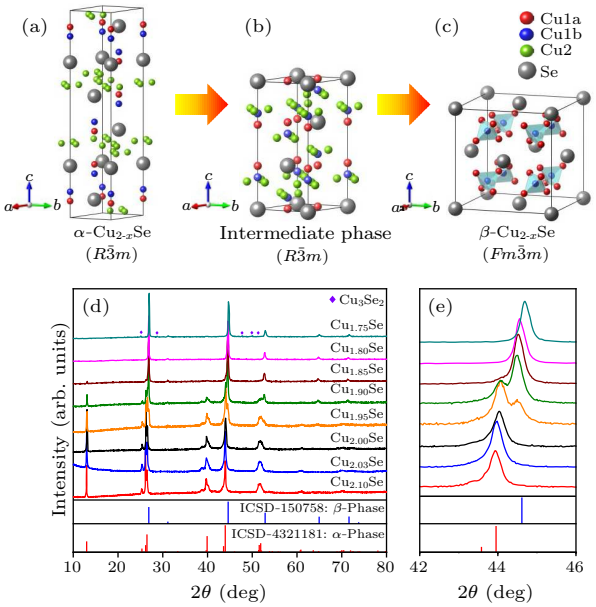

Fig. 1. Crystal structures and x-ray diffraction (XRD) patterns for Cu_xSe. Crystal structures for (a) the low temperature trigonal phase, (b) intermediate phase, and (c) high temperature cubic phase. (d) Room-temperature powder x-ray diffraction (XRD) patterns and (e) enlarged XRD patterns at $2\theta = 42°$–$46°$.

Apart from the crystal structure, the Cu content of Cu_xSe also exerts a significant impact on their phase transition temperature and characters. As shown in Fig. 2(a), a sharp endothermic peak is clearly observed at around 412.7 K in the heat capacity (C_p) curves for the $Cu_{2.10}Se$ sample, corresponding to the phase transition from ordered α-phase to disordered β-phase. The λ-like peak in heat capacity is a signature of second-order phase transition.[28] With decreasing the content of Cu, the critical temperature of phase transition (T_p) is gradually reduced [see Fig. 2(b)]. For $Cu_{1.80}Se$, the T_p is only 281.6 K, which is below the ambient temperature and 131 K lower than that of $Cu_{2.10}Se$. Meanwhile, the intensity of the C_p peak is also gradually weakened with decreasing the amount of Cu content. As shown in Fig. 2(c), the enthalpy change of phase transition (ΔH) for $Cu_{1.80}Se$ is about 3.6 J/g, which is only one ninth of that for $Cu_{2.10}Se$ (33.3 J/g). The reduced ΔH is mainly ascribed to the less content of α-phase in Cu deficient Cu_xSe. The structural transformation is further confirmed by the

high temperature XRD measurements. All the diffraction peaks of Cu_xSe at 450 K can be well indexed to the cubic structure of β-phase [see Fig. 2(d)]. In addition, the diffraction peaks gradually shift to higher 2θ angles, suggesting a shrinkage of unit cells when introducing more Cu vacancies into Cu_xSe. The variation of phase transition characters should have a direct impact on the thermal and electrical transport properties during phase transitions.

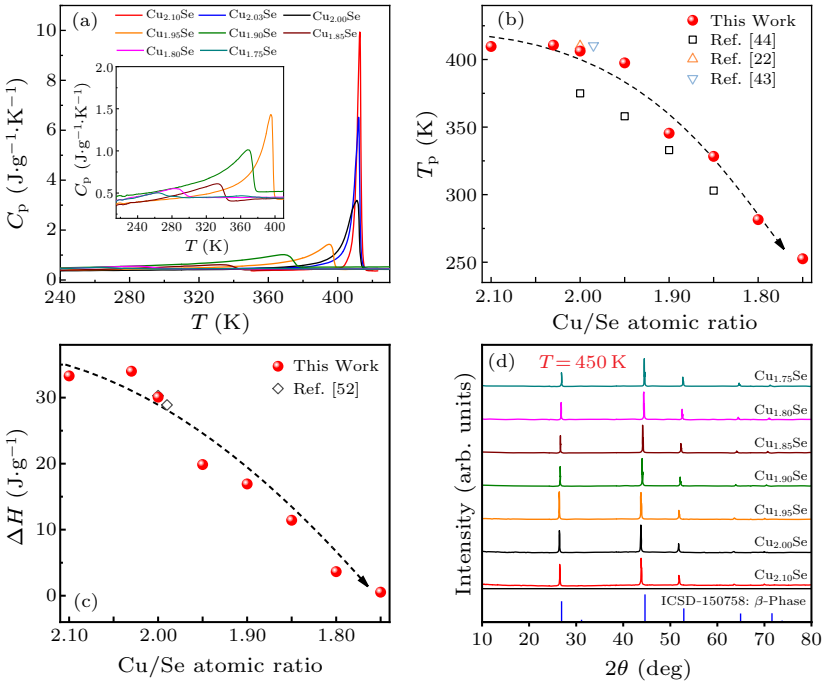

Fig. 2. Phase transition characters for Cu_xSe. (a) Heat capacity measured by the differential scanning calorimetric (DSC) method. (b) Critical temperature T_p as a function of Cu/Se atomic ratio. (c) Phase transition enthalpy ΔH as a function of Cu/Se atomic ratio. The data points of hollow symbols are taken from Refs. [31,43,44,52]. (d) High temperature powder XRD patterns measured at 450 K.

Figure 3 shows the thermal transport properties for Cu_xSe ($x = 2.10$, 2.03, 2.00, 1.95, 1.90, 1.85, 1.80 and 1.75) near room temperature and during phase transitions. Owing to the heat exchange from phase transition, the true thermal diffusivity λ_0 during phase transitions could largely deviate from the the measured thermal diffusivity λ_m. According to Chen *et al.*, the correlation between λ_m and λ_0 could be written as[41]

$$\frac{\lambda_m}{\lambda_0} \approx \frac{1}{1+C_{pt}/C_{p0}} + \frac{C_{pt}/C_{p0}}{1+C_{pt}/C_{p0}} \cdot \exp\left[-\frac{1.81L^2B}{\lambda_0\pi^2}\cdot\frac{1+C_{pt}/C_{p0}}{1}\right],$$

where B is the speed of phase transition, L is the thickness of the material, C_{p0} is the normal heat capacity from the phonons and electrons, $C_{pt} = \Delta H \times \frac{\partial a_{eq}}{\partial T}$ is the equivalent heat capacity arising from phase transitions. As can be seen, λ_m/λ_0 is mainly related to C_{pt}/C_{p0} and B. The term C_{pt}/C_{p0} could be easily derived from the measured heat capacity curves (Fig. S5), while the speed of phase transition B could be obtained by fitting the heat flow curves with different heating rates. The fitting curves and fitting parameters are given in Fig. S6 and Table S2, respectively. Figure 3(a) shows the relationship between phase transition speed B and T/T_p for Cu_xSe ($x = 2.10$–1.95). The obtained B value for $Cu_{2.00}Se$ is around 0.19 s^{-1} during phase transitions, which is decreased to 0.086 s^{-1} and 0.047 s^{-1} for $Cu_{2.10}Se$ and $Cu_{1.95}Se$, respectively. Interestingly, the $Cu_{1.95}Se$ sample shows the lowest speed of phase transition while the activation energy is the lowest ($E \sim 171$ kJ/mol). According to our previous work,[41] the speed of phase transition can be expressed as

$$B = A \cdot n \cdot \exp\left(-\frac{E}{RT}\right) \cdot \frac{(1-a_{eq})^{n-1}}{a_{eq}}.$$

Here, A is the pre-exponential factor related to the mole fraction of high temperature phase, n is the reaction order, E is the activation energy, R is the gas constant, and a_{eq} is the mole fraction of high temperature phase in the equilibrium state. The speed of phase transition, B, is not only related with the activation energy E, but also related with the reaction order and the mole fraction of the high-temperature phase. The $Cu_{2.00}Se$ and $Cu_{2.10}Se$ samples are pure trigonal phases while $Cu_{1.95}Se$ is a mixture of trigonal phase and high-temperature cubic phase. As a result, the obtained A for $Cu_{1.95}Se$ is smaller than

that of $Cu_{2.00}Se$ and $Cu_{2.10}Se$, leading to a lower B in $Cu_{1.95}Se$ though its activation energy E is also low. Nevertheless, these B values are still quite large compared to those in Ag_2S and Ag_2Se.[41] The large B and C_{pt}/C_{p0} imply that λ_m/λ_0 can be significantly lower than 1 and thus the true λ_0 is much higher than the measured λ_m. As shown in Fig. 3(b), the measured minimal thermal diffusivity for $Cu_{2.00}Se$ is $0.072\,mm^2/s$, while the true minimal thermal diffusivity for $Cu_{2.00}Se$ is $0.21\,mm^2/s$. Nevertheless, the thermal diffusivity curves for the $x = 2.10$, 2.03, 2.00, and 1.95 samples still exhibit an obvious dip during phase transitions even though the contribution of heat exchange is removed.

Based on the determined true λ_0, we calculated the thermal conductivity during phase transitions using the equation $\kappa = C_{p0}d\lambda_0$, where d is the sample density. As shown in Fig. 3(c), the κ shows a temperature dependence similar to λ_0. When approaching the critical temperature T_p, the κ values of $Cu_{2.00}Se$, $Cu_{2.03}Se$ and $Cu_{2.10}Se$ are dramatically decreased due to the strong critical scatterings of electron and phonon during second-order phase transitions. A minimal κ of $0.24\,W\cdot m^{-1}\,K^{-1}$ is obtained in $Cu_{2.10}Se$, which is 2.4 times lower than those of normal α-phase and β-phase. With decreasing the Cu/Se atomic ratio, the λ_0 and κ gradually increase during the whole temperature range, which are mainly attributed to the weakened critical scattering and lowered electrical resistivity. The temperature-dependent κ for $Cu_{1.90}Se$ and $Cu_{1.85}Se$ changes smoothly from the mixed phase to single β-phase, which agrees with the character of first-order phase transition.[53] In addition, there is no abrupt change in κ for $Cu_{1.80}Se$ and $Cu_{1.75}Se$ because these samples are single β-phases at room temperature.

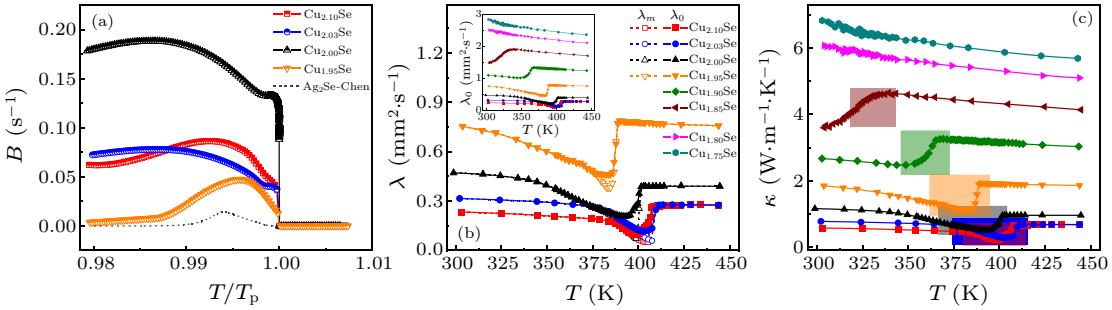

Fig. 3. Thermal transport properties for Cu_xSe near room temperature and during phase transitions. (a) B as a function of T/T_p for the $x = 2.10$, 2.03, 2.00 and 1.95 samples. Here, B refers to the speed of phase transitions. (b) Temperature dependence of measured thermal diffusivity λ_m and corrected thermal diffusivity λ_0. (c) Temperature dependence of thermal conductivity κ calculated from λ_0 and heat capacity C_{p0}. The color regions represent the temperature range of phase transitions.

Figure 4 presents the electrical transport properties for Cu_xSe ($x = 1.75$, 1.80, 1.85, 1.90, 1.95, 2.00, 2.03 and 2.10) near room temperature and during phase transitions. The nominally stoichiometric Cu_2Se is an intrinsic p-type conductor due to the easily formation of Cu vacancies inside the crystal lattices.[35] Each Cu vacancy provides one hole according to the simple electron-counting rule. Experimentally, very high hole concentration with the value around $6 \times 10^{20}\,cm^{-3}$ is usually detected in Cu_2Se[50,54] [see Fig. 4(a)]. Via introducing excess Cu into Cu_xSe ($x > 2.0$), the formation of Cu vacancies can be largely suppressed, leading to a much lower hole concentration in $Cu_{2.10}Se$ ($1.7 \times 10^{20}\,cm^{-3}$). In contrast, the hole concentration p is immensely improved when decreasing the Cu/Se atomic ratio in Cu_xSe. A maximum p of $7 \times 10^{21}\,cm^{-3}$ is obtained in $Cu_{1.75}Se$, which is 40 times higher than that of $Cu_{2.10}Se$. The general increase trend with decreasing Cu content is in accordance with the results from previous studies. Because of the variation of crystal structure and the enhanced scattering by Cu vacancies, the carrier mobility μ is gradually decreased with the decreasing Cu/Se atomic ratio [see Fig. 4(b)].

The electrical transport properties during phase transitions were delicately measured by a home-made system based on the thermal expansion equipment. To authenticate the data, the electrical properties before and after the phase transitions were re-measured using a commercial apparatus ZEM-3. The results are shown in Figs. 4(c)–4(d) and Fig. S2. With decreasing the Cu/Se atomic ratio, the overall ρ and S are greatly enhanced at normal phase regions and during phase transitions owing to the improved hole concentrations. More remarkably, the Cu_xSe samples with different compositions exhibit distinct temperature-dependent transport properties. Both electrical resistivity ρ and Seebeck coefficient S for $Cu_{2.00}Se$, $Cu_{2.03}Se$ and $Cu_{2.10}Se$ are sharply increased when the temperature approaches the critical temperature T_p, while the ρ and S for $Cu_{1.95}Se$ are only slight improved before they drop to the normal value of β-phase. The temperature-dependent ρ and S for $Cu_{1.90}Se$ and $Cu_{1.85}Se$ change continuously and slowly

from the mixed phases to single β-phase. No knee points are observed in the curves of ρ and S for $Cu_{1.80}Se$ and $Cu_{1.75}Se$ because their phase transitions are below room temperature. Figures 4(e) and 4(f) show the net increment of Seebeck coefficient ΔS and electrical resistivity $\Delta\rho$ during phase transitions as a function of Cu/Se atomic ratio. Obviously, both ΔS and $\Delta\rho$ are gradually lowered with decreasing x. The $\Delta\rho$ for $Cu_{2.10}Se$ is around 7.1 Ω·m, which is decreased to 1.6 Ω·m for $Cu_{2.00}Se$ and further decreased to 0.13 Ω·m for $Cu_{1.95}Se$. Similarly, the ΔS for $Cu_{2.10}Se$ is around 31.2 μV/K, which is decreased to 9.2 μV/K for $Cu_{1.95}Se$ and further decreased to nearly zero for $Cu_{1.90}Se$ and other Cu-deficient samples. In addition, it is found that the critical temperature of phase transition is much lowered when decreasing the Cu content, which is coincident with our DSC results.

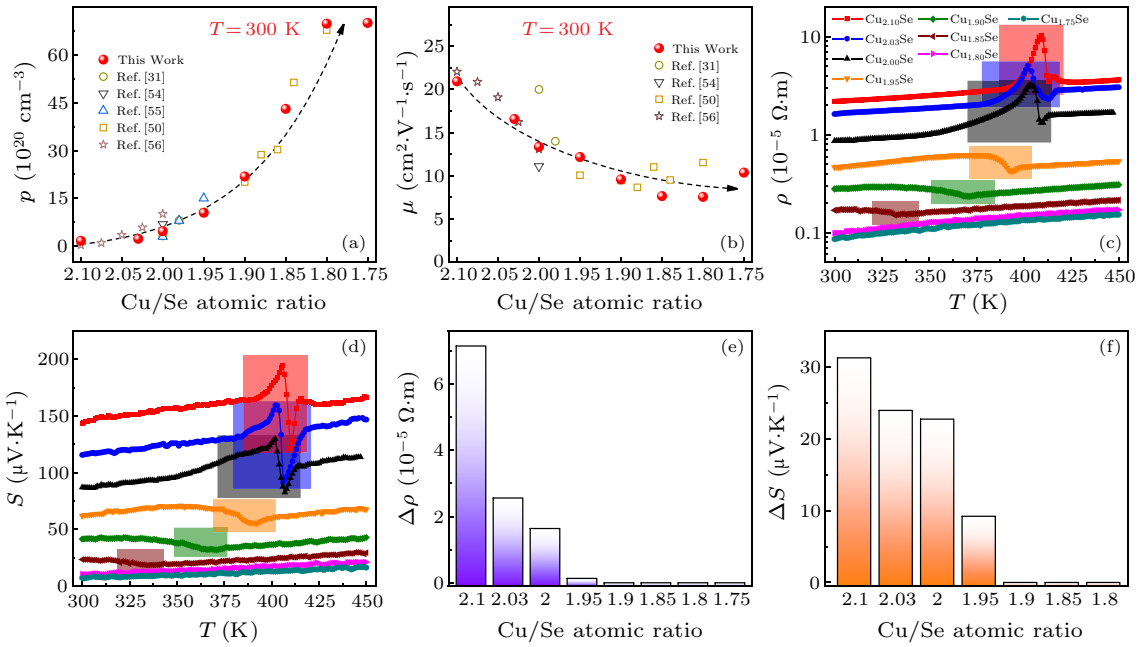

Fig. 4. Electrical transport properties for Cu_xSe near room temperature and during phase transitions. (a) Hall carrier concentration p and (b) carrier mobility μ_H as a function of Cu/Se atomic ratio at 300 K. The data from Refs. [31,50,54–56] are included for comparison. The dashed lines are guide to the eyes. Temperature dependence of (c) electrical resistivity ρ and (d) Seebeck coefficient S. The color regions represent the temperature range of phase transitions. The net increment of (e) electrical resistivity $\Delta\rho$ and (f) Seebeck coefficient ΔS during phase transitions as a function of Cu/Se atomic ratio.

The above results suggest that the variation in chemical compositions changes the characteristic of phase transitions and thus alters the transport behavior during phase transitions. In terms of microscopic mechanism, Seebeck coefficient is the ratio of entropy to charge in the process of carrier transport.[48] Generally, the entropy of charge transport can be divided into two components: one is the net entropy change with the addition of a carrier to the system; the other is the ratio of transported energy to the absolute temperature.[48] Thus, the total Seebeck coefficient is the sum of contributions from these two components, i.e.,

$$S = S_{\text{presence}} + S_{\text{transport}}.$$

Typically, S_{presence} is dominated by the distribution of the carriers in different degenerate energy levels, which is correlated with the electronic structures and electron density of states near Fermi level. $S_{\text{transport}}$, which is associated with the scattering mechanism of charge carriers, is induced by the manner in which charge is transported.[57] During the structural transformation process of Cu_2Se, the structural entropy will dramatically change over a wide temperature range, accompanied by the reconstruction and broadening of energy band. These changes lead to a substantial enhancement in S_{presence}. On the other hand, the fluctuations in sample density, structure, and atomic positions result in strong critical scattering of carriers, which increases the transport entropy of carriers and thereby enhance $S_{\text{transport}}$. As a total result, the Seebeck coefficient S during phase transitions is greatly improved for Cu_2Se. Meanwhile, the critical scattering of carriers reduces the carrier mobility and thus increases the electrical resistivity ρ when the temperature is raised to the critical phase transition point.

With decreasing the Cu content, the phase transition character is modified, and the phase transition enthalpy is lowered, as reflected by our heat capacity analysis. Both the structural entropy and transport

entropy are gradually reduced, leading to a smaller ΔS during phase transitions. Concurrently, the scattering intensity of carriers is also mitigated as the Cu content decreases from 2.10 to 1.75, giving rise to a higher carrier mobility during phase transitions. Therefore, the net increment of electrical resistivity ($\Delta\rho$) is also lowered with decreasing the Cu content.

Benefitting from the extremely low κ and high Seebeck coefficient, the zT values of Cu_xSe samples are substantially improved during phase transitions (see Fig. 5). A maximum zT of 1.38 is achieved at 397 K for $Cu_{2.10}Se$, which represents a 280%–320% improvement over those of normal α-phase and β-phase. Note such a remarkable zT is also one of the highest values recorded below 400 K. With the decreasing Cu/Se atomic ratio, the peak zT is gradually lowered due to the weak critical behaviors and over-high carrier concentrations.

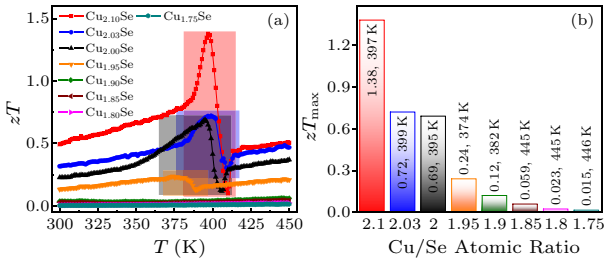

Fig. 5. Figure of merit for Cu_xSe near room temperature and during phase transitions. (a) Dimensionless figure of merit (zT) as a function of temperature for Cu_xSe ($x = 1.75$, 1.80, 1.85, 1.90, 1.95, 2.00, 2.03 and 2.10). The color regions represent the temperature range of phase transitions. (b) The maximum zT during phase transitions as a function of Cu/Se atomic ratio.

In summary, we have successfully synthesized a series of Cu_xSe samples and systematically investigated their crystal structures, chemical compositions, phase transition features, and particularly the electron and phonon transports during phase transitions. The crystal structures and phase transitions of Cu_xSe are very sensitive to the chemical compositions. Cu_xSe ($2.00 \le x \le 2.10$) is single α-phase with trigonal structure; Cu_xSe ($1.90 \le x \le 1.95$) is a mixture of α- and β-phases, while Cu_xSe ($1.75 \le x \le 1.85$) is single β-phase with cubic structure at 300 K. Thanks to the strong critical behaviors of electrons and phonons during phase transitions, a record high zT of 1.38 is obtained at 397 K for $Cu_{2.10}Se$, which is at least 2.8 times larger than that of normal α-phase and β-phase. With the decreasing Cu/Se atomic ratio, the phase transition temperature is gradually reduced, and the phase transition character is altered. Accordingly, the critical behaviors of electrons and phonons during phase transitions are mitigated, resulting in a smaller reduction of κ and a lower increment of ρ and S, as well as a lower zT when decreasing the Cu contents. This work demonstrates that the addition of overs-stoichiometry Cu in Cu_xSe is an effective way to enhance the TE properties during phase transitions.

Data availability. The raw/processed data required to reproduce these findings are available from the corresponding author on reasonable request.

References

[1] Shi X, Chen L and Uher C 2016 *Int. Mater. Rev.* **61** 379
[2] Snyder G J and Toberer E S 2008 *Nat. Mater.* **7** 105
[3] Shi X L, Zou J and Chen Z G 2020 *Chem. Rev.* **120** 7399
[4] Chowdhury I, Prasher R, Lofgreen K, Chrysler G, Narasimhan S, Mahajan R, Koester D, Alley R and Venkatasubramanian R 2009 *Nat. Nanotechnol.* **4** 235
[5] Hudak N S and Amatucci G G 2008 *J. Appl. Phys.* **103** 101301
[6] Sharp J, Bierschenk J and Lyon H B 2006 *Proc. IEEE* **94** 1602
[7] Snyder G J, Lim J R, Huang C K and Fleurial J P 2003 *Nat. Mater.* **2** 528
[8] Zhao H Z, Sui J E, Tang Z J, Lan Y C, Jie Q G, Kraemer D, McEnaney K N, Guloy A, Chen G and Ren Z F 2014 *Nano Energy* **7** 97
[9] Zhang J, Song L, Pedersen S H, Yin H, Hung L T and Iversen B B 2017 *Nat. Commun.* **8** 13901
[10] Mao J, Shuai J, Song S W, Wu Y X, Dally R, Zhou J W, Liu Z H, Sun J F, Zhang Q Y, dela C C, Wilson S, Pei Y Z, Singh D J, Chen G, Chu C W and Ren Z F 2017 *Proc. Natl. Acad. Sci. USA* **114** 10548
[11] Liang J, Qiu P, Zhu Y, Huang H, Gao Z, Zhang Z, Shi X and Chen L 2020 *Research* **2020** 6591981
[12] Shi X, Chen H Y, Hao F, Liu R H, Wang T, Qiu P F, Burkhardt U, Grin Y and Chen L D 2018 *Nat. Mater.* **17** 421
[13] Chen H Y, Wei T R, Zhao K P, Qiu P F, Chen L D, He J and Shi X 2021 *Infomat* **3** 22
[14] Gao Z Q, Yang Q Y, Qiu P F, Wei T R, Yang S Q, Xiao J, Chen L D and Shi X 2021 *Adv. Energy Mater* **11** 2170086
[15] Liang J S, Wang T, Qiu P F, Yang S Q, Ming C, Chen H Y, Song Q F, Zhao K P, Wei T R, Ren D D, Sun Y Y, Shi X, He J and Chen L D 2019 *Energy Environ. Sci.* **12** 2983
[16] Yang S Q, Gao Z Q, Qiu P F, Liang J S, Wei T R, Deng T T, Xiao J, Shi X and Chen L D 2021 *Adv. Mater.* **33** 2007681
[17] He S Y, Li Y B, Liu L, Jiang Y, Feng J J, Zhu W, Zhang J Y, Dong Z R, Deng Y, Luo J, Zhang W Q and Chen G 2020 *Sci. Adv.* **6** eaaz8423
[18] Poudel B, Hao Q, Ma Y, Lan Y C, Minnich A, Yu B, Yan X A, Wang D Z, Muto A, Vashaee D, Chen X Y, Liu J M, Dresselhaus M S, Chen G and Ren Z F 2008 *Science* **320** 634
[19] Zhai R S, Wu Y H, Zhu T J and Zhao X B 2018 *Rare Met.* **37** 308
[20] Witting I T, Chasapis T C, Ricci F, Peters M, Heinz N A, Hautier G and Snyder G J 2019 *Adv. Electron. Mater.* **5** 1800904
[21] Mao J, Chen G and Ren Z F 2021 *Nat. Mater.* **20** 454
[22] Liu H L, Shi X, Kirkham M, Wang H, Li Q, Uher C, Zhang W Q and Chen L D 2013 *Mater. Lett.* **93** 121
[23] Jiang B, Qiu P, Chen H, Huang J, Mao T, Wang Y, Song Q, Ren D, Shi X, Chen L 2018 *Mater Today Phys.* **5** 20
[24] Lu P, Qiu W J, Wei Y Y, Zhu C X, Shi X, Chen L D and Xu F F 2020 *Acta Crystallogr. Sect. B-Struct. Sci. Cryst. Eng. Mat.* **76** 201
[25] Chen L C, Chen P Q, Li W J, Zhang Q, Struzhkin V V, Goncharov A F, Ren Z F and Chen X J 2019 *Nat. Mater.* **18** 1321

[26] Mahan G D 2015 *J. Appl. Phys.* **117** 045101
[27] Sun S, Li Y, Chen Y, Xu X, Kang L, Zhou J, Xia W, Liu S, Wang M, Jiang J, Liang A, Pei D, Zhao K, Qiu P, Shi X, Chen L, Guo Y, Wang Z, Zhang Y, Liu Z, Yang L and Chen Y 2020 *Chin. Sci. Bull.* **65** 1888
[28] Liu H L, Yuan X, Lu P, Shi X, Xu F F, He Y, Tang Y S, Bai S Q, Zhang W Q, Chen L D, Lin Y, Shi L, Lin H, Gao X Y, Zhang X M, Chi H, Uher C 2013 *Adv. Mater.* **25** 6607
[29] Zhao K, Eikeland E, He D *et al.* 2021 *Joule* **5** 1183
[30] Yang L, Chen Z G, Han G, Hong M, Zou Y C, Zou J 2015 *Nano Energy* **16** 367
[31] Liu H, Shi X, Xu F, Zhang L, Zhang W, Chen L, Li Q, Uher C, Day T and Snyder G J 2012 *Nat. Mater.* **11** 422
[32] Liu Y Y, Qiu P F, Chen H Y, Chen R, Shi X and Chen L D 2017 *J. Inorg. Mater.* **32** 1337
[33] Qiu P, Shi X and Chen L 2016 *Energy Storage Mater.* **3** 85
[34] Zhang Z, Zhao K, Wei T R, Qiu P, Chen L and Shi X 2020 *Energy Environ. Sci.* **13** 3307
[35] Zhao K, Blichfeld A B, Chen H, Song Q, Zhang T, Zhu C, Ren D, Hanus R, Qiu P, Iversen B B, Xu F, Snyder G J, Shi X and Chen L 2017 *Chem. Mat.* **29** 6367
[36] Zhao K, Qiu P, Shi X and Chen L 2020 *Adv. Funct. Mater.* **30** 1903867
[37] Zhao K P, Qiu P F, Song Q F, Blichfeld A B, Eikeland E, Ren D D, Ge B H, Iversen B B, Shi X and Chen L D 2017 *Mater. Today Phys.* **1** 14
[38] Yang D W, Su X L, Li J, Bai H, Wang S Y, Li Z, Tang H, Tang K C, Luo T T, Yan Y G, Wu J S, Yang J H, Zhang Q J, Uher C, Kanatzidis M G and Tang X F 2020 *Adv. Mater.* **32** 2003730
[39] Deng T T, Wei T R, Huang H, Song Q F, Zhao K P, Qiu P F, Yang J, Chen L D and Shi X 2020 *npj Comput. Mater.* **6** 81
[40] Bai H, Su X L, Yang D W, Zhang Q J, Tan G J, Uher C, Tang X F and Wu J S 2021 *Adv. Funct. Mater.* **31** 2100431
[41] Chen H, Yue Z, Ren D, Zeng H, Wei T, Zhao K, Yang R, Qiu P, Chen L and Shi X 2018 *Adv. Mater.* **31** 1806518
[42] Eikeland E, Blichfeld A B, Borup K A, Zhao K, Overgaard J, Shi X, Chen L and Iversen B B 2017 *IUCrJ.* **4** 476
[43] Kang S D, Danilkin S A, Aydemir U, Avdeev M, Studer A and Snyder G J 2016 *New J. Phys.* **18** 013024
[44] Xiao X X, Xie W J, Tang X F and Zhang Q J 2011 *Chin. Phys. B* **20** 087201
[45] Byeon D, Sobota R, Delime-Codrin K, Choi S, Hirata K, Adachi M, Kiyama M, Matsuura T, Yamamoto Y, Matsunami M and Takeuchi T 2019 *Nat. Commun.* **10** 72
[46] Brown D R, Heijl R, Borup K A, Iversen B B, Palmqvist A, Snyder G J 2016 *Phys. Status Solidi-Rapid Res. Lett.* **10** 618
[47] Liu W D, Yang L, Chen Z G and Zou J 2020 *Adv. Mater.* **32** 1905703
[48] Brown D R, Day T, Borup K A, Christensen S, Iversen B B and Snyder G J 2013 *APL Mater.* **1** 052107
[49] Wang H, Porter W, Bottner H, Konig J, Chen L, Bai S, Tritt T, Mayolett A, Senawiratne J, Smith C, Harris F, Sharp J, Lo J, Kleinke H and Kiss L 2011 *Annex VIII—Thermoelectric Materials for Waste Heat Recovery: An International Collaboration for Transportation Applications* (Oak Ridge: ORNL Press) chap 4 p 14
[50] Yu J, Zhao K, Qiu P, Shi X and Chen L 2017 *Ceram. Int.* **43** 11142
[51] Heyding R D 1966 *Can. J. Chem.* **44** 1233
[52] Chrissafis K, Paraskevopoulos K M, Manolikas C 2006 *J. Therm. Anal.* **84** 195
[53] Duan J L, Zhu C X, Guan M J, Lu P, He Y, Fu Z Q, Zhang L L, Xu F F, Shi X and Chen L D 2018 *Ceram. Int.* **44** 13076
[54] Yang L, Chen Z G, Han G, Hong M and Zou J 2016 *Acta Mater.* **113** 140
[55] Su X L, Fu F, Yan Y G, Zheng G, Liang T, Zhang Q, Cheng X, Yang D W, Chi H, Tang X F, Zhang Q J and Uher C 2014 *Nat. Commun.* **5** 4908
[56] Tak J Y, Nam W H, Lee C, Kim S, Lim Y S, Ko K, Lee S, Seo W S, Cho H K, Shim J H, Park C H 2018 *Chem. Mater.* **30** 3276
[57] Emin D 1999 *Phys. Rev. B* **59** 6205

Supplementary Material for

Enhanced Thermoelectric Properties of Cu_xSe ($1.75 \leq x \leq 2.10$) during Phase Transitions

Zhongmou Yue(岳仲谋)[1,2], Kunpeng Zhao(赵琨鹏)[3,**], Hongyi Chen(陈弘毅)[4], Pengfei Qiu(仇鹏飞)[1,2], Lidong Chen(陈立东)[1,2], and Xun Shi(史迅)[1,2,**]

[1]State Key Laboratory of High Performance Ceramics and Superfine Microstructure, Shanghai Institute of Ceramics, Chinese Academy of Sciences, Shanghai 200050, China

[2]Center of Materials Science and Optoelectronics Engineering, University of Chinese Academy of Sciences, Beijing 100049, China

[3]State Key Laboratory of Metal Matrix Composites, School of Materials Science and Engineering, Shanghai Jiao Tong University, Shanghai 200240, China

[4]College of Chemistry and Chemical Engineering, Central South University, Changsha, Hunan, 410083, China

[**]Corresponding author. Email: zkp.1989@sjtu.edu.cn; xshi@mail.sic.ac.cn.

Calculation of thermal conductivity during the phase transition[1]

The thermal diffusivity measured by laser flash method is calculated from the specimen thickness and the time required for the rear face temperature rise to reach a percentage of its maximum value[1], this could be expressed using equation S1.

$$\lambda = 0.13879 * L^2 * \frac{1}{t_{1/2}} \quad \text{(S1)}$$

Here, λ is the thermal diffusivity, L is the thickness of the sample and $t_{1/2}$ is the half-rise time which represents the time required from the initiation of the plus for the rear face temperature to reach half ΔT_{max}. During a phase transition, extra energy is absorbed from the heat flow to change the crystal structure, the half-rise time of a material during phase transitions could be overlooked. Then the measured thermal diffusivity calculated using equation S1 is underestimated, which should be corrected before further calculation.

To calculate the real thermal conductivity κ during the phase transition, the true λ_0 and C_{p0} without the contribution of phase transition should be used.

$$\kappa_{\text{Real}} = C_{p0} * d * \lambda_0 \quad \text{(S2)}$$

The general heat conduction expression for one-dimensional phase transition is[2]

$$\frac{\kappa}{C_{p0}d}\cdot\frac{\partial^2 T}{\partial x^2}-\frac{\partial T}{\partial t}-\frac{\Delta H}{C_{p0}}\cdot\frac{\partial a}{\partial t}=0 \qquad \text{(S3)}$$

The third term in equation S3 is the energy change due to the phase transition[3]. The temperature dependent mole fraction of high temperature β-phase (a) using the phase transition kinetics equations is given by

$$\frac{da}{dt}=B\cdot(a_{eq}-a) \qquad \text{(S4)}$$

$$B=A\cdot n\cdot\exp(-\frac{E}{RT})\cdot\frac{(1-a_{eq})^{n-1}}{a_{eq}} \qquad \text{(S5)}$$

Here, B refers to the speed of the phase transition, which could be obtained by fitting the heat flow curves with different heating rates. The fitting curves and fitting parameters are given in **Figure S**6 and **Table S**2, respectively. With equations S4 and S5, we can use the phase transition speed B to solve equation S3.

$$B\cdot(\frac{\kappa}{C_{p0}d}\frac{\partial^2 T}{\partial x^2}-\frac{1+C_{pt}/C_{p0}}{1}\frac{\partial T}{\partial t})+\frac{\kappa}{C_{p0}d}\frac{\partial^3 T}{\partial x^2\partial t}-\frac{\partial^2 T}{\partial t^2}=0 \qquad \text{(S6)}$$

Based on equation S6, the approximate solution of the relationship between λ_0 and λ_m is:

$$\frac{\lambda_m}{\lambda_0}\approx\frac{1}{1+C_{pt}/C_{p0}}+\frac{C_{pt}/C_{p0}}{1+C_{pt}/C_{p0}}\cdot e^{-\frac{1.81\cdot B\cdot L^2}{\lambda_0\cdot\pi^2}\cdot\frac{1+C_{pt}/C_{p0}}{1}} \qquad \text{(S7)}$$

Then the true κ during phase transitions could be solved using equation S2.

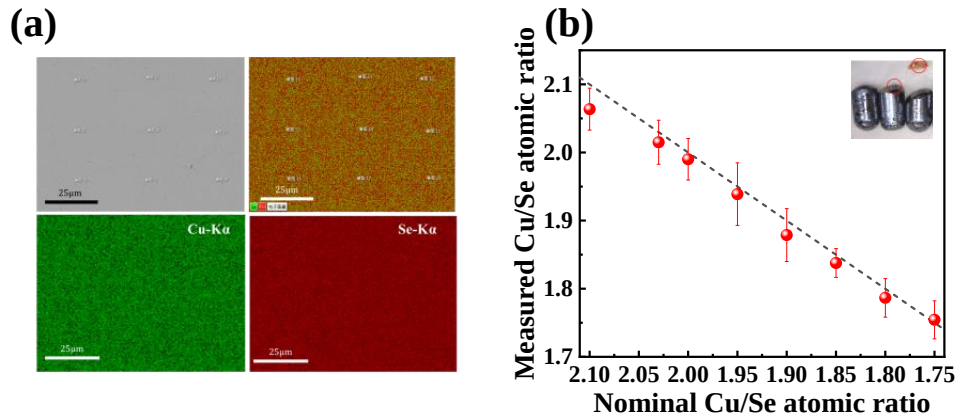

Figure S1. **(a)** Secondary electron (SE) image and elemental energy dispersive spectroscopy (EDS) mapping for Cu_2Se. **(b)** Nominal Cu/Se atomic ratio *vs* measured Cu/Se atomic ratio for Cu_xSe (x=1.75, 1.80, 1.85, 1.90, 1.95, 2.00, 2.03 and 2.10) samples. 9 points are randomly selected to obtain the mean value and the error bar is shown in the figure. The inset shows the ingots after annealing.

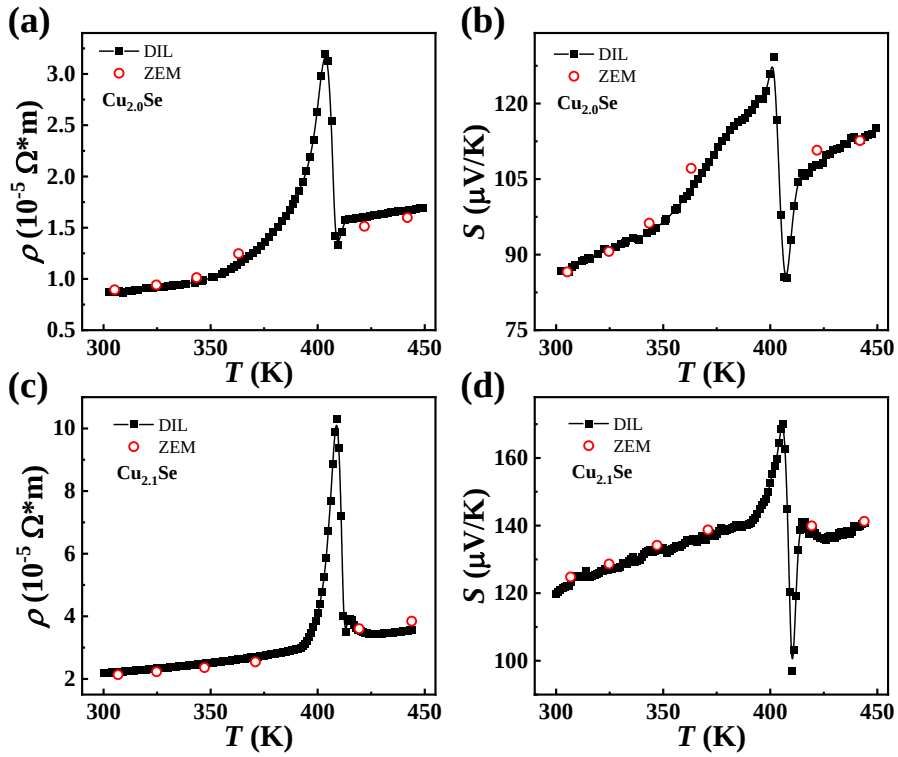

Figure S2. Electrical resistivity (ρ) and Seebeck coefficient (S) measured by DIL (black square) and ULVAC ZEM-3 system (red circle) for $Cu_{2.00}Se$ and $Cu_{2.10}Se$

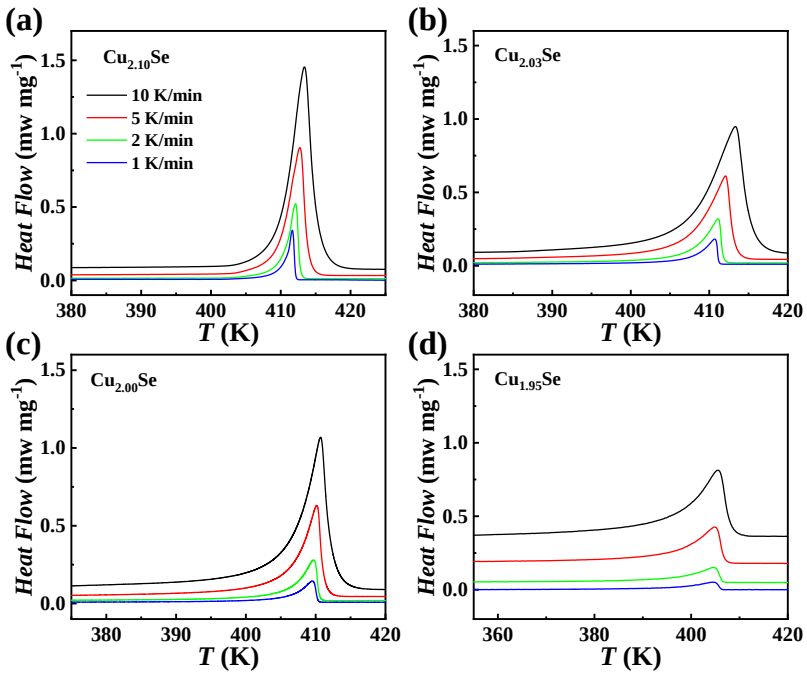

Figure S3. Heat flow curves for $Cu_{2.10}Se$, $Cu_{2.03}Se$, $Cu_{2.00}Se$ and $Cu_{1.95}Se$ measured by DSC with different heating rates (1.0, 2.0, 5.0 and 10 K/min).

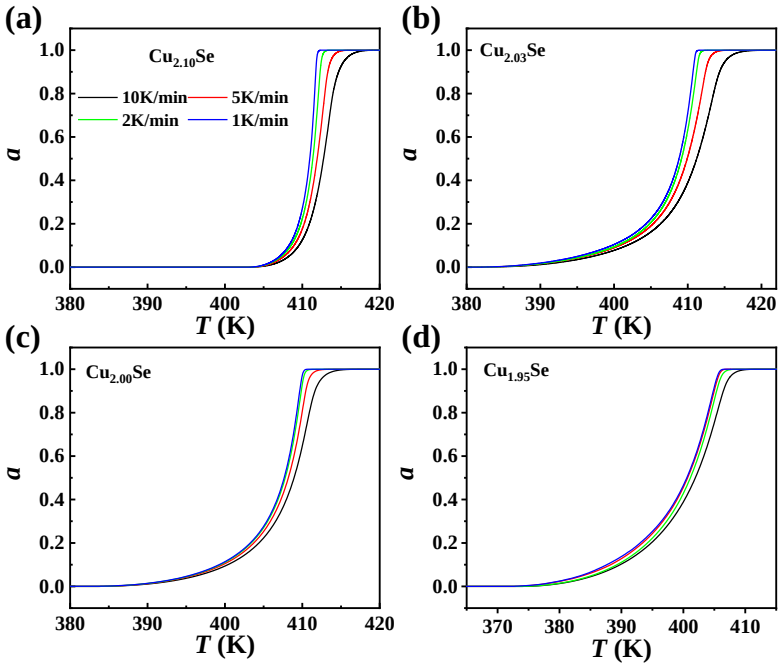

Figure S4. Temperature dependence of mole fraction of high temperature β-phase at different heating rates (1.0, 2.0, 5.0 and 10 K/min) for **(a)** $Cu_{2.10}Se$, **(b)** $Cu_{2.03}Se$ **(c)** $Cu_{2.00}Se$ and **(d)** $Cu_{1.95}Se$.

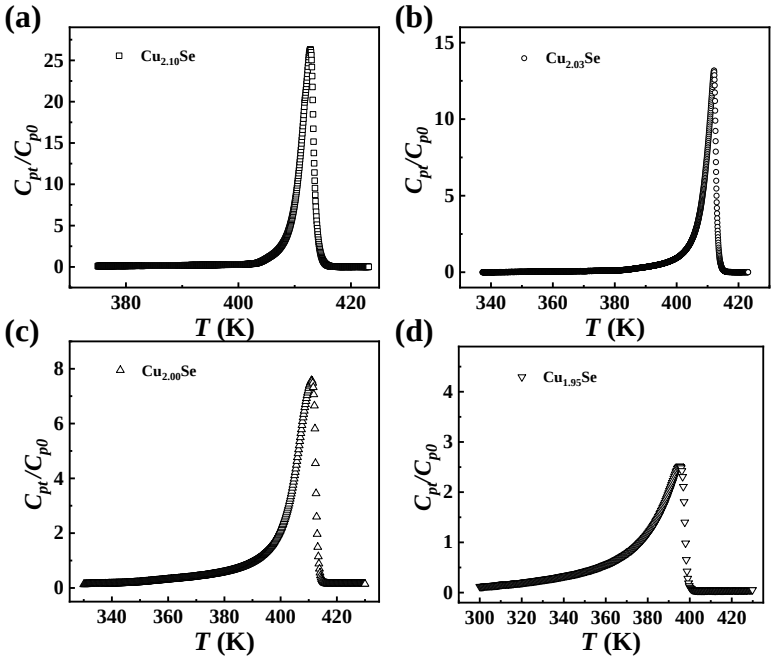

Figure S5. C_{pt}/C_{p0} for Cu_xSe ($1.95 \leq x \leq 2.10$) during the phase transition. The heat capacity is measured with a heating rate of 5 K min^{-1}.

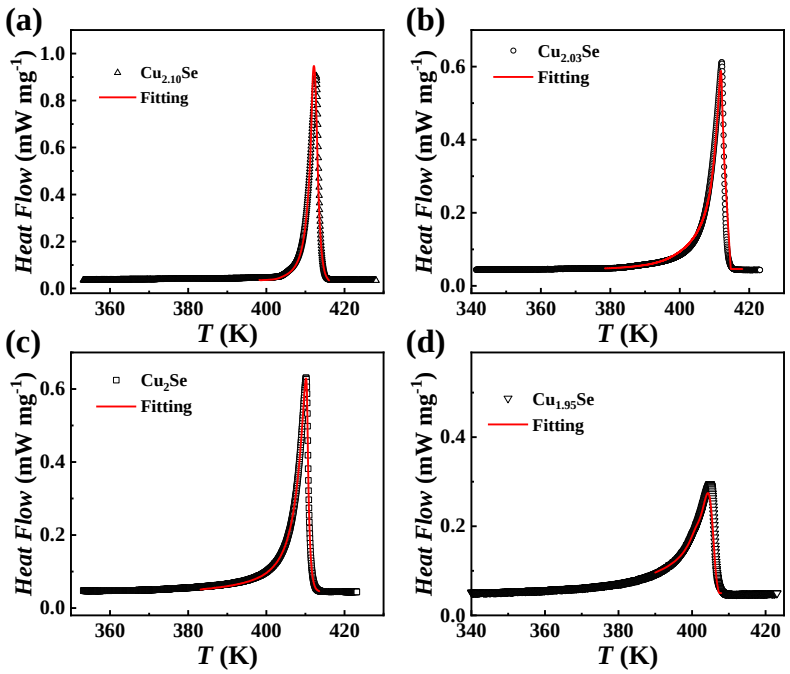

Figure S6. Heat Flow measured with a heating rate of 5 K min^{-1}. The symbols represent the experiment data, and the red lines are fitted by the equations S3 and S4 with the fitting parameters listed in **Table S**2

Table S1. The critical temperature T_p measured with a heating rate of 1 K min^{-1} and the offset of critical temperature ΔT_p measured with heating rates of 2 K min^{-1}, 5 K min^{-1}, and 10 K min^{-1} for Cu_xSe (x =1.85, 1.90, 1.95, 2.00, 2.03 and 2.10) samples.

Materials	T_p **(K)**	ΔT_p **(K)**		
	1K min^{-1}	**2K min^{-1}**	**5K min^{-1}**	**10K min^{-1}**
$Cu_{2.10}Se$	411.65	0.5	1.1	1.9
$Cu_{2.03}Se$	410.70	0.4	1.4	2.6
$Cu_{2.00}Se$	409.45	0.3	0.6	1.2
$Cu_{1.95}Se$	404.45	0.2	0.4	1.1
$Cu_{1.90}Se$	376.25	0.3	0.6	1.2
$Cu_{1.85}Se$	362.55	-0.1	0.0	0.1

Table S2. DSC Fitting parameters using phase transition kinetics equations S3 and S4. n is the reaction order, A is the pre-exponential factor, E is the activation energy.

Materials	E **[kJ mol^{-1}]**	***Log(A)***	***n-1***
$Cu_{2.10}Se$	636	79	0.078
$Cu_{2.03}Se$	253	31	0.065
$Cu_{2.00}Se$	247	30	0.024
$Cu_{1.95}Se$	171	28	0.097

References

[1]. Astm E 1991 *Annual book of ASTM standards* **15**, 750

[2]. Chen H, Yue Z, Ren D, Zeng H, Wei T, Zhao K, Yang R, Qiu P, Chen L, Shi X 2018 *Adv. Mater.* **31**

[3]. Incropera F P, DeWitt D P, Bergman T L, Lavine A S *Fundamentals of heat and mass transfer* 1996 (New York: Wiley Press)